Salt Stress in *Desulfovibrio vulgaris* Hildenborough: an Integrated Genomics Approach

Aindrila Mukhopadhyay,[1,2] Zhili He,[1,4] Eric J. Alm,[1,2] Adam P. Arkin,[1,2,7] Edward E. Baidoo,[1,2]
Sharon C. Borglin,[1,3] Wenqiong Chen,[1,6] Terry C. Hazen,[1,3] Qiang He,[1,4] Hoi-Ying Holman,[1,3]
Katherine Huang,[1,2] Rick Huang,[1,3] Dominique C. Joyner,[1,3] Natalie Katz,[1,3] Martin Keller,[1,6]
Paul Oeller,[1,6] Alyssa Redding,[1,7] Jun Sun,[1,6] Judy Wall,[1,5] Jing Wei,[1,6] Zamin Yang,[1,4]
Huei-Che Yen,[1,5] Jizhong Zhou,[1,4] and Jay D. Keasling[1,2,7]*

Virtual Institute of Microbial Stress and Survival[1]†; *Physical Biosciences Division, Lawrence Berkeley National Laboratory,
Berkeley, California*[2]; *Earth Sciences Division, Lawrence Berkeley National Laboratory, Berkeley, California*[3];
Environmental Sciences Division, Oak Ridge National Laboratory, Oak Ridge, Tennessee[4]; *Biochemistry and
Molecular Microbiology & Immunology Departments, University of Missouri, Columbia, Missouri*[5];
Diversa Inc., San Diego, California[6]; *and Departments of Chemical Engineering and
Bioengineering, University of California, Berkeley, California*[7]

The ability of Desulfovibrio vulgaris Hildenborough to reduce, and therefore contain, toxic and radioactive metal waste has made all factors that affect the physiology of this organism of great interest. Increased salinity is an important and frequent fluctuation faced by *D. vulgaris* in its natural habitat. In liquid culture, exposure to excess salt resulted in striking elongation of *D. vulgaris* cells. Using data from transcriptomics, proteomics, metabolite assays, phospholipid fatty acid profiling, and electron microscopy, we used a systems approach to explore the effects of excess NaCl on *D. vulgaris*. In this study we demonstrated that import of osmoprotectants, such as glycine betaine and ectoine, is the primary mechanism used by *D. vulgaris* to counter hyperionic stress. Several efflux systems were also highly up-regulated, as was the ATP synthesis pathway. Increases in the levels of both RNA and DNA helicases suggested that salt stress affected the stability of nucleic acid base pairing. An overall increase in the level of branched fatty acids indicated that there were changes in cell wall fluidity. The immediate response to salt stress included up-regulation of chemotaxis genes, although flagellar biosynthesis was down-regulated. Other down-regulated systems included lactate uptake permeases and ABC transport systems. The results of an extensive NaCl stress analysis were compared with microarray data from a KCl stress analysis, and unlike many other bacteria, *D. vulgaris* responded similarly to the two stresses. Integration of data from multiple methods allowed us to develop a conceptual model for the salt stress response in *D. vulgaris* that can be compared to those in other microorganisms.

Originally isolated in 1946 from clay soils in Hildenborough, Kent, United Kingdom, *Desulfovibrio vulgaris* Hildenborough belongs to the sulfate-reducing class of bacteria that are ubiquitous in nature (23, 45). These anaerobes generate energy by reducing sulfate (42) and play important roles in global sulfur cycling and complete mineralization of organic matter. *D. vulgaris* has been implicated in biocorrosion of oil and gas pipelines both on land and in the ocean (5, 23, 57). Members of this species have also been found to reduce metals in sediments and soils with high concentrations of NaCl and a milieu of toxic metals (6) and to cope with salt stresses that result from environmental hydration-dehydration cycles. An understanding of the ability of *D. vulgaris* to survive in the presence of high concentrations of NaCl and osmotic stress is critical for determining the biogeochemistry at metal-contaminated sites for bioremediation and natural attenuation and for predicting the potential for biocorrosion of pipelines and tanks in soils, sediments, and off-shore oil production facilities (8, 38, 62). The availability of an annotated genomic sequence for *D. vulgaris*

makes this organism ideal for studying the complex physiology of sulfate-reducing bacteria (25).

The bacterial response to hyperionic stress includes a range of mechanisms, such as aquaporins for water intake and functions regulated by the stationary-phase sigma factor, RpoS (12, 53). A commonly encountered response is accumulation of neutral, polar, small molecules, such as glycine betaine (GB), proline, trehalose, or ectoine (20, 29, 33). These compatible solutes serve as osmoprotectants and are synthesized and/or imported into the cell. The genomic sequence of *D. vulgaris* provides insight into its potential responses to increased salt in the environment. While genes for trehalose synthesis (*otsBA*) are present in the closely related microbe *Desulfovibrio* sp. strain G20, homologues are not present in *D. vulgaris*. Furthermore, no genes for ectoine synthesis or transport can be identifed. *D. vulgaris* does contain genes for proline biosynthesis and an ABC transport system annotated for the uptake of GB, choline, and proline.

Compared to the responses to hyperionic stress, the responses specific to Na^+ stress are less understood, since they are often observed in conjunction with responses to osmotic or alkaline stress (15). RpoS-regulated genes have also been found to be responsive to Na^+ stress (12, 19). Also often implicated are Na^+/H^+ antiporters, such as those encoded by

the *nha* genes in *Escherichia coli* (15, 56), orthologs of which are present in *D. vulgaris*.

A comprehensive understanding of various stress response mechanisms requires the use of multiple techniques to examine changes in different types of biomolecules. Integrated analyses involving a combination of microarray data and proteomics are increasingly being used for studies at a cellular level. Although mRNA and protein levels are linked, additional regulation during and after translation requires that expression at both stages be monitored for a more complete view of the physiological landscape (3, 24, 40). Although not addressed here, critical information concerning cellular proteomic responses also lies in posttransalational modifications. In this study, changes in the transcript and protein levels were examined. The data sets obtained were complemented by the results of a preliminary metabolite analysis. In addition, phospholipid fatty acid (PLFA) composition and lipid content, which are measures of changes in cell membrane properties, were also studied.

MATERIALS AND METHODS

Culture maintenance. *D. vulgaris* Hildenborough (ATCC 29579) was obtained from the American Type Culture Collection (Manassas, VA). For all experiments and culture maintenance we used a defined lactate sulfate medium (LS4D medium) based on Postgate's medium C (50). One liter of LS4D medium (pH 7.2) contains 50 mM NaSO$_4$, 60 mM sodium lactate, 8 mM MgCl$_2$, 20 mM NH$_4$Cl, 2.2 mM K$_2$PO$_4$, 0.6 mM CaCl$_2$, 30 mM piperazine-*N*,*N*'-bis(ethanesulfonic acid) (PIPES) buffer, 640 μl of resazurin (0.1% solution), 10 mM NaOH, 1 ml of Thauers vitamins (10), 12.5 ml of trace minerals (10), and 5 ml of titanium citrate. To prepare titanium citrate, 500 ml of 0.2 M sodium citrate was boiled for 20 min under a continuous stream of nitrogen to remove dissolved oxygen. While the preparation was hot, 37.5 ml of 20% (wt/vol) TiCl$_3$ was added along with 100 ml of 8% (wt/vol) Na$_2$CO$_3$ under nitrogen. The final mixture was autoclaved and used. Subculturing was minimized by using −80°C *D. vulgaris* stocks as 10% inocula for 100- to 200-ml fresh LS4D medium starter cultures at the mid-log phase of growth (optical density at 600 nm [OD$_{600}$], 0.3 to 0.4). These cultures were then used as 10% inocula for 1- to 3-liter production cultures. All cultures were grown at 30°C.

MIC. MIC was defined as the stressor concentration that doubled the generation time and/or decreased the overall yield by 50%. Growth curve experiments were conducted in 96-well plates using an OmniLog instrument (Biolog Inc., Hayward, CA), which captured digital optical density images every 15 min for 150 h. Each well was inoculated with 10% mid-log-phase cells, six replicates of each stressor dilution were used, and the plates were placed in an anaerobic atmosphere and sealed in airtight Retain bags (Nasco) before they were placed in the OmniLog. OmniLog measurements were calibrated against *D. vulgaris* cell densities obtained by determining the OD$_{600}$, using a Biolog plate reader (OD$_{590}$), and determining direct cell counts by the acridine orange direct count method. All growth curves were comparable at 95% confidence intervals for the exponential growth phase. A kinetic plot of *D. vulgaris* growth was used to determine the generation time and cell yield. For NaCl and KCl stress, the MIC for *D. vulgaris* was determined to be 250 mM (in addition to the concentration present in LS4D medium) by testing concentrations ranging from 0 to 5,000 mM. For all experiments in this study, 250 mM NaCl or KCl was added to growth medium to establish stress conditions.

Biomass production. Highly controlled and reproducible conditions were used for simultaneous production of cell cultures for transcriptomics, proteomics, metabolite assay, PLFA, and synchrotron Fourier transform infrared (sFTIR) spectromicroscopy studies. Control and experimental production cultures were prepared in triplicate. Cultures were exposed to stress at the mid-log phase to minimize in-culture variability. NaCl or KCl (250 mM) was added to experimental cultures, and an equivalent volume of sterile distilled water was added to control cultures. The time of stressor addition was defined as zero time, and samples were taken at 30, 60, 120, and 240 min after exposure. The longest time (<5 h) was less than one generation time, so all samples were collected prior to the stationary phase. Samples were chilled to 4°C in <15 s during collection by pulling samples from production cultures through 7 m of capillary tubing immersed in an ice bath using a peristaltic pump. Chilled samples were centrifuged,

and pellets were washed with 4°C degassed sterile phosphate-buffered saline and centrifuged again at 6,000 × *g* (10 min, 4°C). The final pellet was flash frozen in liquid N$_2$ and stored at −80°C. For the production of each biomass sample, the following purity and growth characteristics were recorded: temperature, pH, OD$_{600}$, acridine orange direct count, sFTIR spectrum, total protein content, anaerobic colony morphology, absence of aerobic colonies, and PLFA biosignatures.

Osmoprotection assays. *D. vulgaris* was cultured anaerobically in LS4D medium. Stressors, osmolytes, and other metabolites were added as indicated below, and growth was monitored by determining the OD$_{600}$ and the total cell protein content.

Microarray analysis. Oligonucleotide probe design and microarray construction have been described previously (34). After RNA extraction, purification, and labeling, a reverse transcription reaction was used to generate labeled cDNA probes. Labeled genomic DNA (Cy3) was used as a control and as the common reference to cohybridize with labeled RNA (Cy5) samples for each slide. Each comparison was done in triplicate. Finally, since there were duplicate arrays on a given slide and three biological replicates, there were a total of 18 possible spots for each gene. Hybridized microarray slides were scanned using the ScanArray Express microarray analysis system (Perkin-Elmer, Massachusetts). Spot signals, spot quality, and background fluorescence intensities were quantified with ImaGene, version 5.5 (Biodiscovery Inc., Los Angeles, CA). For raw microarray data see NCBI GEO accession number GSE4447.

Computational. (i) Gene models. Models of The Institute for Genomic Research (NCBI) were used.

(ii) Microarray data analysis. Log expression levels, including global normalization, were first computed for each microarray. Log expression levels obtained from replicate arrays were averaged. Each gene was represented by two spots on each microarray, and spots flagged by the scanning software were excluded. The net signal of each spot was calculated by subtracting the background signal and adding a pseudosignal of 100 to obtain a positive value. For resulting net signals of <50, a value of 50 was used. For each spot, the level of expression was the ratio of the two channels (ratio of mRNA to genomic DNA). For each replicate, the levels were normalized so that the total expression levels for the spots that were present on all replicates were identical. Finally, mean expression levels and standard deviations of each spot were calculated, which required *n* > 1. To estimate differential gene expression in control and treatment conditions, normalized log ratios were used. The log ratio was log$_2$(treatment) − log$_2$(control). This log ratio was normalized using LOWESS on the difference versus the sum of the log expression level (16). Sector-based artifacts were observed; therefore, the log ratio was further normalized by subtracting the median of all spots within each sector. Up to this point, data were processed using spots instead of genes to allow sector-based normalization. Finally, the spots for each gene were averaged to obtain a final normalized log ratio. To assess the significance of the normalized log ratio, a *Z* score was calculated by using the following equation:

$$Z = \frac{\log_2(\text{treatment/control})}{\sqrt{0.25 + \Sigma\text{variance}}}$$

where 0.25 is a pseudovariance term. Log ratios and *Z* values for all microarray data in this study are listed in a supplemental data file (http://vimss.lbl.gov/SaltStress/). The log ratios and *Z* values were used to generate two types of plots, (i) volcano plots and (ii) operon-based estimates of local accuracy. For volcano plots, we plotted the log$_2$ ratio of all genes versus *Z* . This provided an estimate of the total numbers of significant changers in a microarray comparison and allowed determination of which time showed the most changers (http://vimss.lbl.gov/SaltStress/). For operon-based estimates of local accuracy, each point represented a group of 100 predicted significant changers with similar *Z* scores (the point showed the least significant *Z* value in the set). The estimated accuracy of each group of changers was derived by inspecting other genes in the same operon as these changers. For random changers, the transcripts for 50% of these genes should have been regulated in the same direction, and for perfect changers 100% of the genes should have been regulated in the same direction. Members of the operons without a consistent signal across replicates (*Z* < 0.5) were excluded. Even with perfect microarray data, the estimated accuracy was somewhat less than 100% due to errors in operon predictions. Typically, a cutoff *Z* value of >2 provided accurate significant changers. For operon plots see http://www.microbesonline.org/cgi-bin/microarray/viewExp.cgi?expId = 14,20,33.

Metabolite assays using CE-MS. Three identical 50-ml cultures were pooled anaerobically and centrifuged at 10,000 × *g* (10 min, 4°C). The pellet was resuspended in 5 ml cold methanol (prechilled on dry ice) by vortexing and allowed to stand for 5 min on dry ice. A mixture of 5 ml chloroform (Acros) and 2 ml water was added to the lysate, and the preparation was mixed thoroughly to
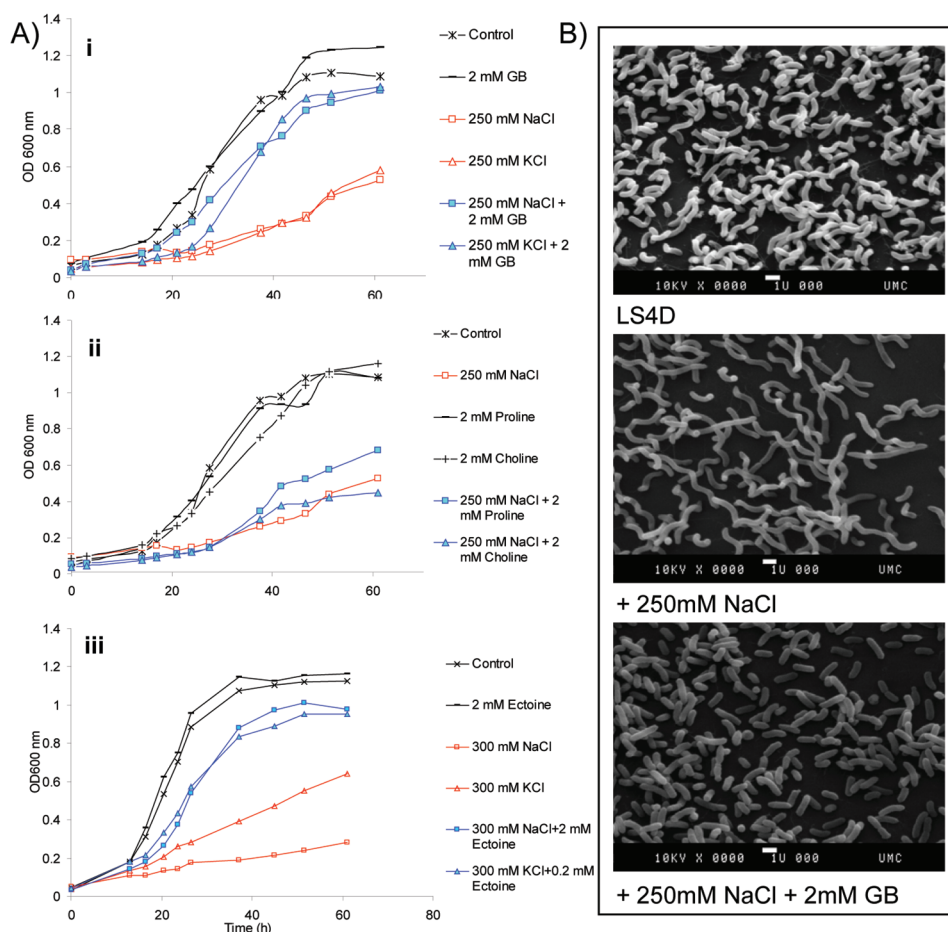
FIG. 1. Effect of salt stress on growth and cell morphology of *D. vulgaris* and role of osmoprotectants. (A) (Panel i) Effect of 250 mM additional NaCl or KCl on the growth of *D. vulgaris* in LS4D medium and effect of the presence of 2 mM GB during salt stress; (panel ii) effect of proline and choline on NaCl-stressed cells; (panel iii) effect of ectoine on NaCl- or KCl-stressed cells. Linear plots were used for ease of visualizing the effects of the different growth conditions on the biomass. Log plots are available at http://vimss.lbl.gov/SaltStress/. (B) Scanning electron microscopy images of *D. vulgaris* grown in different conditions (Electron Microscopy Core, University of Missouri, Columbia).

remove free phospholipids. The extraction mixture was centrifuged at 7,000 × *g* for 5 min to separate the aqueous and nonaqueous layers. The top layer was transferred to a 5,000-molecular-weight-cutoff filter (Vivaspin6) and centrifuged at 7,000 × *g* (10 min, 4°C). The filtrate was lyophilized and reconstituted in 4 ml water. For desalting, solid-phase extraction (1g C$_{18}$ cartridge; (Varian) was used. The C$_{18}$ cartridge was conditioned using 4 ml methanol, followed by 4 ml water. The reconstituted sample (4 ml) was introduced into the cartridge and washed with 4 ml of water to remove salts. The sample was eluted with 4 ml methanol to which enough water was added for the sample to remain frozen at −80°C, and it was lyophilized (Labconco). Dried samples were reconstituted to produce metabolite mixtures in 100 μl buffer containing 115 μM methionine sulfone as the internal standard. Data were obtained in the positive ion mode by capillary electrophoresis (CE) (Agilent) and were analyzed using electrospray mass spectrometry (MS) (Agilent MSD). The metabolite mixture was resolved on a fused silica column (1 m by 50 μm; Polymicro Technologies) with 1 M formic acid as the electrolyte and 5 mM ammonium acetate as the sheath liquid. Metabolites were identified by comparing the nominal mass and retention time with the nominal masses and retention times of standards. Quantities of selected metabolites were estimated by comparison with known quantities of internal standards. All reagents used were high-performance liquid chromatography grade (Honey Well Burdick and Jackson).

ICAT and tandem liquid chromatography-mass spectrometry (LC-MS). To obtain total cell protein, cell pellets from 300-ml cultures at OD$_{600}$ of 0.3 to 0.4 were lysed in 2 ml of 50 mM Tris-HCl (pH 8.0) by sonication on ice. The lysates were clarified by centrifugation at 14,000 × *g* (30 min, 4°C), and protein levels were determined using the bicinchoninic acid assay (Pierce). Samples (300 μg) of total cell protein from control and stressed samples (120 min) were labeled by isotope-coded affinity tagging (ICAT) with light and heavy tags, respectively, according to the manufacturer's instructions (Applied Biosystems). Trypsinized samples were desalted by using a C$_{18}$ macro spin column (The Nest Group, Inc., Massachusetts) according to the manufacturer's instructions. Each sample was dried using a Speedvac (Thermo Savant), dissolved in 40 μl of 0.1% (vol/vol) 1 M formic acid, resolved by two-dimensional nano liquid chromatography (LC) using an inline strong cation-exchange cartridge into salt cuts (5, 20, 30, 40, 50, and 1,000 mM KCl), and resolved further by reverse-phase separation (15-cm 300-Å-diameter C$_{18}$ RP column; Dionex). A 0 to 30% gradient in the organic phase (80% acetonitrile, 0.1% 1 M formic acid) was used. The *m/z* values of the resolved peptides were determined using electrospray ionization and a time of flight mass spectrometer (QSTAR hybrid quadrupole time of flight mass spectrometer; Applied Biosystems). Time of flight MS and MS-MS results were analyzed using the ProICAT software (Applied Biosystems). The acquired data were searched against a theoretical database created using the FASTA file containing the open reading frames of *D. vulgaris* Hildenborough, *E. coli* K-12, and *Bacillus subtilis* 168. A mass tolerance of 0.3 for MS and a mass tolerance of 0.3 for MS-MS were used to obtain a list of candidate proteins. The database of results generated by ProICAT computed the ID confidence for all peptides identified and the quantitation quality for ICAT peptide pairs for which a heavy/light ratio could be determined. Quantitation quality ranges from 0 to 100 and is based on how well the mass difference of the ICAT pair agrees with the expected value. Only proteins identified at >99% confidence were used. Of these proteins, only those with a stressed/control (heavy/light) quantitation quality of >75% were used. The ICAT strategy has been determined to be very accurate

for small changes, detecting as little as a 30% change in protein levels (3, 61). Heavy/light ratios for peptides associated with the same protein were used to assess the internal error in a manner similar to the manner described previously (22). Internal error refers to the error between technical replicates of the same ICAT-labeled sample examined twice by LC-MS as described above. The error was determined to be 29%, and therefore, only changes greater than 29% were considered significant. The complete list is available at http://vimss.lbl.gov /SaltStress/.

Three-dimensional nano LC-MS proteomics. For the three-dimensional proteomics analysis, performed at Diversa Corp., we used fractionation of total proteins by three-dimensional LC, followed by MS-MS analysis to identify the proteins, as described previously (59). Replicate cultures from a control (time zero and 120 min) and a stressed sample (120 min) were used to obtain total protein. The relative abundance of proteins in each sample was estimated based on the hypothesis that the more abundant a peptide ion is in a mixture, the more likely the peptide ion is sampled during the course of an MS-MS experiment (35, 61). When this model is used, the total numbers of qualified spectral counts represent the relative abundance of each protein under a specific condition. To identify proteins for which there were significant changes under different conditions, the statistical "local-pooled-error" test (28) was used. Only changers with a P value of <0.05 were considered to be significantly changed. A total of 1,356 proteins were identified in all samples, and for 47 of these proteins there were reproducible changes between the control and the stressed sample (http://vimss .lbl.gov/SaltStress/).

PLFA assays. Pellets from 40-ml cultures (centrifuged at $1,015 \times g$ for 15 min) were stored at $-20°C$. Total lipids were extracted from each pellet with a modified Bligh-Dyer solution (60). Phospholipids were separated from total lipids on a C_{18} silicic acid column (Unisil; Clarkson Chemical), methylated, and then analyzed with an Agilent 6890N gas chromatograph equipped with a flame ionization detector. Peaks were confirmed by MS (Agilent 5972A MSD), and double bond positions were confirmed by dimethyl disulfide derivatization. Peaks were quantified using an internal 19:0 fatty acid methyl ester standard (Sigma).

sFTIR spectromicroscopy. All sample handling was done anaerobically at 4°C. Cells were washed in ice-cold, oxygen-free buffer (0.1 M Tris-HCl [pH 7.5], 1.0 mM EDTA) and placed on a gold-coated microscope slide. The free-flowing buffer solution was removed, and cells were placed inside a sample holder, which maintained a relative humidity of 100% and an anaerobic atmosphere. The ZnSe window of the sample holder allowed acquisition of infrared spectra. Infrared measurements were obtained at the Advanced Light Source Facility, Lawrence Berkeley National Laboratory, using an Fourier transform infrared interferometer bench (Nicolet Magna 760) equipped with an infrared microscope (Nic-Plan IR microscope), as described previously (27). Signals in the spectral region from 4,000 to 250 cm^{-1} were interpreted using previously described principles (9). Characteristic CO_2 peaks and water vapor fingerprints were removed from the spectra, and the resulting spectra were normalized against the amide I absorption peak (1,648 cm^{-1}). Each spectrum was the average of 20 raw spectra, and each raw spectrum represented at least 20 cells. Differences in spectra, which revealed differences in cellular changes in control and stressed biomasses, were analyzed.

RESULTS AND DISCUSSION

The defined LS4D medium used in our study contains sodium lactate as a carbon source and electron donor and sodium sulfate as an terminal electron acceptor. An additional 250 mM NaCl reduced the maximal growth rate of the *D. vulgaris* culture by 50% and resulted in a striking phenotype, fivefold elongation of cells in the late log phase (Fig. 1).

In this study, *D. vulgaris* cultures in the mid-log phase were exposed to salt stress using 250 mM NaCl, and changes in gene expression were monitored after 30, 60, 120, and 240 min, using genomic DNA as a control. The highest number of changers were seen at 120 min (http://vimss.lbl.gov/SaltStress/), and therefore a replicate 120-min experiment was conducted to generate biomass for a microarray analysis, a proteomics analysis, metabolite assays, and a macromolecule composition analysis. The resulting data were used to delineate primary cellular responses to excess NaCl. Data from an identical KCl
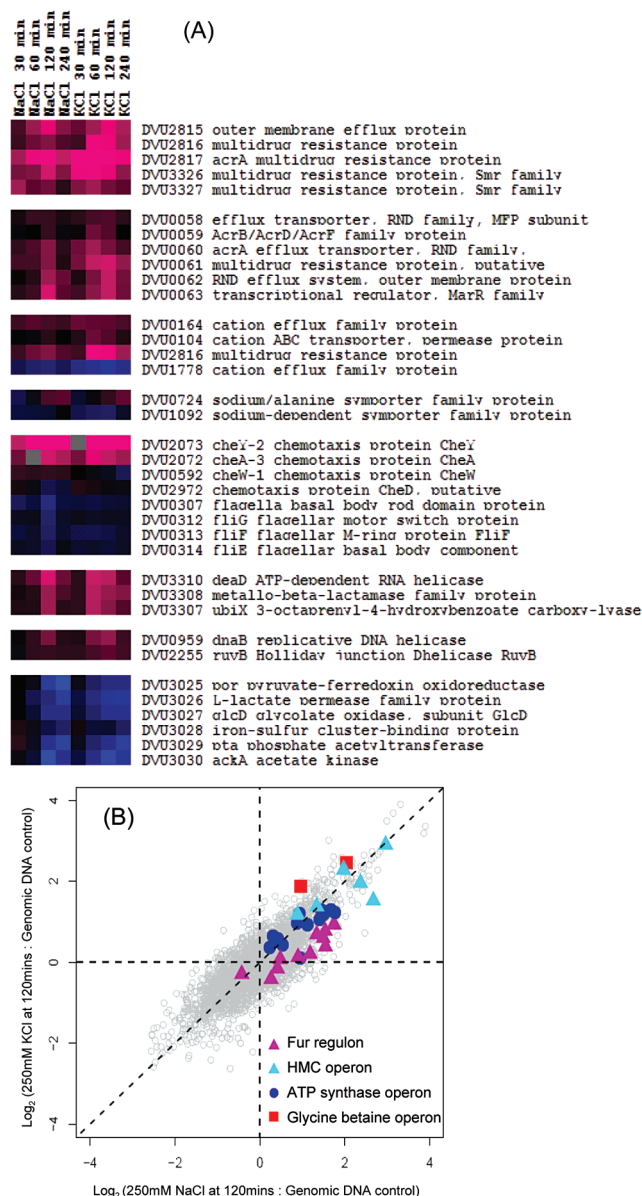

FIG. 2. (A) Selected hits from the NaCl and KCl microarrays. The color blocks show changes in mRNA levels for selected *D. vulgaris* genes over time in response to both NaCl stress and KCl stress, as follows: pink, increase; blue, decrease; black, no change; gray, data not available. Genes are grouped by function or gene identification numbers, and the groups do not indicate clustering. (B) Comparison of NaCl and KCl stress responses: plot of changes in mRNA levels with 250 mM KCl stress (120 min) (*y* axis) versus changes in mRNA levels with 250 mM NaCl stress (120 min) (*x* axis). The data show the large overlap in the mRNA changes in response to KCl and NaCl. The plot shows the similarity between the KCl and NaCl stress responses. Points in the top right quadrant represent increases in both data sets. Values on both axes are log_2 values for the ratio of the mRNA level under stressed conditions to the control genomic DNA. Since for both microarrays genomic DNA was used as the control, such a direct comparison could be made. Data for selected candidate operons and regulons, including the FUR and Hmc regulons, the ATP biosynthesis operon, and the glycine betaine uptake operon, are highlighted.

TABLE 1. Selected microarray data: log$_2$ ratios for 250 mM NaCl versus no NaCl and for 250 mM KCl versus no KCl at 120 min[a]

DVU no.	Designation	Description	Log$_2$ ratio (Z value)	
			NaCl	KCl
Glycine betaine uptake operon				
DVU2297	*proW*	Glycine betaine/L-proline ABC transporter, periplasmic binding protein	1.62 (3.13)	1.87 (3.68)
DVU2298	*opuBB*	Glycine betaine/L-proline ABC transporter, permease protein	1.43 (2.74)	2.53 (4.91)
DVU2299	*proV*	Glycine betaine/L-proline ABC transporter, ATP-binding protein	1.48 (2.56)	2.47 (4.63)
Sulfate reduction pathway				
DVU0846	ApsB	Adenylylsulfate reductase, beta subunit	0.64 (1.21)	0.50 (0.99)
DVU0847	ApsA	Adenylylsulfate reductase, alpha subunit	0.71 (1.31)	0.23 (0.44)
DVU0848	QmoA	Quinone-interacting membrane-bound oxidoreductase	0.82 (1.41)	0.61 (1.18)
DVU0849	QmoB	Quinone-interacting membrane-bound oxidoreductase	1.20 (2.12)	0.59 (1.04)
DVU0850	QmoC	Quinone-interacting membrane-bound oxidoreductase	0.55 (1.07)	0.11 (0.18)
DVU0279	NA[b]	Sulfate permease family protein	0.86 (1.66)	1.85 (3.41)
Potassium transport				
DVU1606	NA	Potassium uptake protein, TrkA family	0.02 (0.05)	−0.21 (−0.39)
DVU3335	NA	Sensory box histidine kinase	−0.64 (−1.17)	−1.30 (−2.44)
DVU3336	*kdpD*	Potassium channel histidine kinase domain protein	−0.75 (−1.43)	−0.56 (−1.01)
DVU3337	*kdpC*	Potassium-transporting ATPase, C subunit	−0.04 (−0.06)	0.35 (0.61)
DVU3338	*kdpB*	Potassium-transporting ATPase, B subunit	0.24 (0.42)	0.41 (0.70)
DVU3339	*kdpA*	Potassium-transporting ATPase, A subunit	0.48 (0.79)	−0.07 (−0.12)
DVU0412	NA	Potassium uptake protein TrkA, putative	0.31 (0.55)	0.42 (0.81)
DVU0413	*trk1*	Potassium uptake protein, TrkH family	0.51 (1.00)	0.76 (1.46)
Sigma factors				
DVU1584	*rpoH*	Sigma-70 family protein	−0.10 (−0.19)	0.13 (0.25)
DVU1628	*rpoN*	RNA polymerase sigma-54 factor	1.05 (1.88)	0.66 (1.19)
DVU1788	*rpoD*	RNA polymerase sigma-70 factor	0.24 (0.43)	0.30 (0.55)
DVU2929	*rpoC*	DNA-directed RNA polymerase, beta prime subunit	0.68 (1.32)	0.76 (1.32)
DVU3229	*fliA*	RNA polymerase sigma factor for flagellar operon FliA	−0.01 (−0.02)	(NA)
Lactate permeases				
DVU2110	b2975	l-Lactate permease	−0.75 (−1.43)	−0.44 (−0.82)
DVU2285	NA	l-Lactate permease family protein	0.12 (0.21)	−0.37 (−0.71)
DVU2451	NA	l-Lactate permease family protein	−1.36 (−2.54)	−2.29 (−4.42)
DVU2683	NA	l-Lactate permease family protein	−0.28 (−0.48)	−1.29 (−2.48)
DVU3026	NA	l-Lactate permease family protein	−1.93 (−3.72)	−1.77 (−3.31)
DVU3284	b2975	l-Lactate permease	−0.05 (−0.08)	−0.36 (−0.63)

[a] Genes are sorted by DVU numbers within subgroups. log$_2$ ratios and Z values were computed as described in Materials and Methods.
[b] NA, not applicable.

stress analysis were used to identify responses that may be specific to excess Na$^+$ ions.

Accumulation of compatible solutes. The *D. vulgaris* genome encodes a putative GB-choline-proline ABC transport system. The three-gene operon contains *proV*, encoding an ATP-binding protein; *opuBB*, encoding a permease protein; and *proW*, encoding the periplasmic binding protein that serves as the substrate receptor in the transporter complex. Microarray analysis showed that the mRNA levels of all three genes were highly up-regulated in response to both excess NaCl and KCl (Fig. 2B and Table 1). ICAT proteomics data for the same biomass supported the *opuBB* up-regulation (Fig. 3), and OpuBB was among the mostly highly up-regulated proteins.

Surprisingly, even though no GB is present in LS4D medium, analysis of cell extracts using CE-MS showed that GB was present in both control biomass and salt-stressed biomass. Consistent with both microarray and proteomics observations, the GB levels were higher in salt-stressed biomass (Fig. 3). Bacteria are known to scavenge GB present as a contaminant
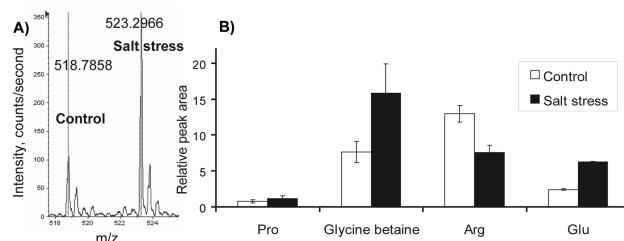

FIG. 3. (A) ICAT proteomics data for the glycine betaine permease OpuBB: section of the time of flight MS spectrum showing the light (control) and heavy (NaCl-stressed) ICAT ion pair for the peptide FTCLGIR. The FTCLGIR sequence was obtained at 99% confidence from MS-MS of the parent ion at *m/z* 523.29 (or a molecular mass of 1,046.59 Da) and was used to identify OpuBB (DVU2298). The +2 charged parent ion peaks, separated by *m/z* 4.5, were used for relative peak quantification using ProICAT. The stressed/control ratio of 3.45 is consistent with up-regulation of OpuBB. (B) Quantities of selected metabolites relative to the quantity of the internal standard (defined as 100%). The bars indicate averages for three technical replicates.

in carbon sources (20). Alternatively, *D. vulgaris* may be able to synthesize GB from other precursors. For instance, LS4D medium contains choline, which can serve as a precursor of GB in a two-step process that requires an aldehyde dehydrogenase and an alcohol dehydrogenase (11), genes for which are present in *D. vulgaris*, although microarray data did not identify any specific candidates.

In osmoprotection assays, very low concentrations of GB not only efficiently alleviated the growth inhibition due to excess salt but also prevented the late-log-phase cell elongation (Fig. 1). While this indicates that GB is an effective osmoprotectant, the up-regulated permease encoded by *opuBB* may not be specific to GB. Hence, additional substrates known to be effective osmoprotectants or precursors of GB were also tested. Our results showed that choline did not alleviate salt stress in *D. vulgaris* (Fig. 1). This may have been due to either the inability of *D. vulgaris* to import choline or the absence of specific dehydrogenases that convert choline to GB. GB has also been reported to be synthesized via sequential methylation of the glycine amino group by methyltransferases (44). Although several methyltransferases have been annotated in *D. vulgaris*, addition of glycine, methyl glycine (sarcosine), or dimethyl glycine to salt-stressed cells resulted in no significant improvement in growth (http://vimss.lbl.gov/SaltStress/). Organisms that use GB as an osmoprotectant, including *E. coli* and *B. subtilis*, often can synthesize it (11, 20). However, similar to *Lactobacillus* spp. (20), *D. vulgaris* may use GB exclusively via import.

The up-regulation of the GB-choline-proline ABC transport system also suggests that proline is a candidate for osmoprotection in *D. vulgaris*. Proline, a well-documented osmoprotectant (4, 11), may also accumulate due to up-regulation of biosynthesis, increased transport, or decreased proline oxidation to glutamate. Up-regulation of proline biosynthesis genes was not observed upon salt stress (http://vimss.lbl.gov/SaltStress/). Furthermore, CE-MS analysis indicated that cells did not accumulate proline during salt stress, while glutamate levels did increase (Fig. 3). In osmoprotection assays, proline did alleviate salt stress, but not as effectively as GB (Fig. 1). Therefore, despite the homology between the *B. subtilis* and *D. vulgaris opuBB* genes, proline appears not to be the preferred osmoprotectant for *D. vulgaris*.

In contrast, ectoine alleviated salt stress at concentrations comparable to the concentration of GB (Fig. 1). Interestingly, neither an ectoine biosynthesis pathway nor any ectoine-specific transport systems have been annotated in *D. vulgaris*, although it is evident that uptake and accumulation of small polar osmolytes are major salt stress responses in *D. vulgaris*.

Among other amino acids, the mRNA levels of tryptophan biosynthesis genes were markedly up-regulated during NaCl stress and, to a lesser extent, during KCl stress (http://vimss.lbl.gov/SaltStress/). We found no reports of tryptophan up-regulation in relation to salt or osmotic stress in other bacteria and have no explanation for this phenomenon. To investigate if the up-regulation at the transcript level indicated that there was a tryptophan requirement during salt stress, an osmoprotection assay was performed. However, addition of tryptophan did not alleviate the reduction in growth in the presence of 250 mM salt (http://vimss.lbl.gov/SaltStress/).

Efflux of excess salt ions. *D. vulgaris* contains more than 14 genes annotated for cation/multidrug efflux that may pump cations out of the cell using the same mechanism as Na^+/H^+ antiporters. Genes in a three-gene operon (DVU2815 to DVU2817), as well as genes in a two-gene multidrug efflux operon (DVU3326 and DVU3327), were highly up-regulated upon salt stress (Fig. 2). Transcripts of a putative *acrAB* system (DVU0058 to DVU0063) were highly up-regulated throughout the stress treatment in response to both NaCl and KCl (Fig. 2), a phenomenon also observed in *E. coli* in response to 0.5 M NaCl (39). The large number of up-regulated genes with cation/multidrug efflux domains suggests that efflux systems may play a major role in actively pumping excess salt ions out of the cell in *D. vulgaris*.

Several highly conserved Na^+/H^+ antiporters are also present in *D. vulgaris*, but for most of these antiporters the transcript and protein profiles indicated that there was no change in stressed cells (http://vimss.lbl.gov/SaltStress/). While this may indicate that under the conditions studied *D. vulgaris* does not recruit Na^+/H^+ antiporters to exclude excess salt ions, the transcripts of these open reading frames were abundant (Huang and Alm, unpublished observations), adequate levels of the antiporters may be present for salt efflux, and no further up-regulation may be required. One exception was the ubiquinone oxidoreductase subunit, encoded by *echA* (DVU0434), whose transcript levels were increased in the presence of both NaCl-stressed cells (at 120 min, $Z = 2.12$) and KCl-stressed cells (at 120 min, $Z = 2.14$). While no other gene in the operon showed a significant change (http://vimss.lbl.gov/SaltStress/), oxidoreductases such as EchA have been implicated in respiration-coupled Na^+ efflux in several other bacteria (46, 49), and the observed DVU0434 up-regulation may be important in *D. vulgaris* salt stress.

The down-regulated genes included the genes involved in Na^+ uptake, such as the genes encoding flagellar systems (Fig. 2), suggesting that *D. vulgaris* eventually becomes nonmotile under salt stress conditions. Similar down-regulation of the flagellar assembly genes has been observed in other bacteria, including *Shewanella oneidensis* (36) and *B. subtilis* (55). However, unlike *S. oneidensis* cells, the *D. vulgaris* cells were observed to be highly motile after salt stress (data not shown), and several key chemotaxis genes, such as *cheY* (DVU2073), were very highly and reproducibly up-regulated within 30 min of treatment with either NaCl or KCl (Fig. 2A). While *cheY* remained up-regulated throughout the later times monitored, other chemotaxis genes (*cheA*, *cheW*, and *cheD*) were most highly up-regulated only at earlier times (30 and 60 min) (Fig. 2A). The up-regulation of the transcript levels of chemotaxis genes may indicate an initial response in cells to move away from the stressful cations.

At the proteome level several periplasmic-binding proteins of ABC transport systems were significantly down-regulated (Table 2). While both proteomics techniques used in our study revealed this down-regulation, only one of the genes showed a similar change at the mRNA level (DVU1937; $Z = -1.72$). Whether the down-regulation of these periplasmic proteins is beneficial during salt stress requires further investigation.

Salt stress amelioration mechanisms. The most-up-regulated protein identified in the salt-stressed sample in both proteomics data sets was the RNA helicase, DVU3310 (Table 2), a

TABLE 2. Selected proteomic data

DVU no.[a]	Designation	Description	ICAT $\log_2$ ratio (stressed/control)[b]	Three-dimensional nano LC-MS/MS[c]	
				$\log_2$ ratio (stressed/control)	P value
ATP synthesis					
DVU0775	*atpD*	ATP synthase, F1 beta subunit	**1.03**	−0.11	0.8
DVU0777	*atpA*	ATP synthase, F1 alpha subunit	**0.58**	0.40	0.35
DVU0778	*atpH*	ATP synthase, F1 delta subunit	**0.74**	−0.64	0.29
ABC transport binding proteins					
DVU0712	NA[d]	Amino acid ABC transporter, periplasmic binding protein	**−1.41**	**−1.79**	**0.00**
DVU0745	NA	ABC transporter, periplasmic substrate-binding protein	**−0.81**		
DVU1937	NA	ABC transporter, periplasmic phosphonate-binding protein, putative	**−1.17**	**−1.23**	**0.01**
DVU2342	NA	Amino acid ABC transporter, periplasmic amino acid-binding protein	**−1.07**	**−2.05**	**0.01**
DVU0547	NA	Branched-chain amino acid ABC transporter, periplasmic binding protein	**−1.33**	**−1.28**	**0.028**
Sulfate reduction					
DVU0847	ApsA	Adenylylsulfate reductase, alpha subunit	**0.57**	0.17	0.68
DVU0848	QmoA	Quinone-interacting membrane-bound oxidoreductase	0.21	−0.25	0.55
DVU0849	QmoB	Quinone-interacting membrane-bound oxidoreductase	**0.63**	0.23	0.59
Pyruvate → acetate					
DVU3025	*poR*	Pyruvate-ferredoxin oxidoreductase	0.48	0.05	0.90
DVU3027	*glcD*	Glycolate oxidase, subunit GlcD	−0.40	−0.26	0.55
DVU3028	NA	Iron-sulfur cluster-binding protein	−0.02	**−1.71**	**0.00**
DVU3029	*pta*	Phosphate acetyltransferase	−0.06	−0.66	0.13
DVU3030	*ackA*	Acetate kinase	−0.35	−0.78	0.07
DVU3032	NA	Conserved hypothetical protein	0.06	**−0.96**	**0.03**
Selected changers					
DVU3310	*deaD*	ATP-dependent RNA helicase, DEAD/DEAH family	**2.24**	**3.08**	**0.00**
DVU2370	*ompH*	Outer membrane protein OmpH, putative	**0.64**	−1.03	0.23
DVU3242	*rpoZ*	DNA-directed RNA polymerase, omega subunit	**0.66**	2.32	0.61
DVU0697	*rfbA*	Mannose-1-phosphate-guanylyltransferase/mannose-6-phosphate isomerase	**0.75**	−0.50	0.59
DVU2929	*rpoC*	DNA-directed RNA polymerase, beta prime subunit	**0.58**	0.64	0.18
DVU0832	NA	Tetrapyrrole methylase family protein	**−2.65**	−7.64	0.052
DVU2013	NA	Hybrid cluster protein	**−0.61**	**−1.37**	**0.002**
DVU0979	b1200	DAK1 domain protein	**−0.75**	**−1.87**	**0.005**

[a] DVU descriptions can be found at microbesonline.org (2).
[b] For ICAT proteomics the identification confidence is >99% and the quantitation scores are >75% for the data shown. Changes of >29% are significant (indicated by boldface type).
[c] Three-dimensional nano LC-MS/MS proteomics was used to estimate the quantity of protein by spectral counting; P values of <0.05 are indicated by boldface type.
[d] NA, not applicable.

DeaD/DeaH box binding protein known to facilitate RNA melting (18). The remaining genes of the three-gene operon encoding DVU3310 also showed an increase in mRNA levels (Fig. 2A). RNA and DNA helicases are both known confer tolerance to salt (48, 52), presumably by overcoming the effect of excess intracellular cations on RNA and DNA melting. There were also increases in the transcript levels for two DNA helicases, encoded by *dnaB* and *ruvB* (Fig. 2A). Both DnaB and RuvB are predicted to form part of the DNA replication fork and to assist in DNA melting (30). Given the function of these helicases, up-regulation of the transcript levels suggests that the stability of both RNA and DNA may have been affected by excess cations during salt stress.

Salt stress is known to affect the fluidity of the cell wall, and lipid regulation plays a role in cell wall fluidity (37). Eight PLFAs accounting for 80% of the total *D. vulgaris* PLFA com-

position (17) were used to study the effect of NaCl stress on the PLFA profile (Fig. 4). Since our study did not address the long-term adaptation to salt stress, no drastic changes were observed in either the total PLFA content or the net contribution of each individual PLFA (http://vimss.lbl.gov /SaltStress/). However, changes that were observed during salt stress were not observed in the control biomass over the same period of time (Fig. 4). The level of the branched, unsaturated PLFA i17:1w9c, which accounted for 14% of the total PLFA content and is characteristic of *Desulfovibrio* species (17), increased in stressed cells but not in control cells. In contrast, the levels of the unbranched, saturated PLFAs 16:0 (7%) and 18:0 (25%) decreased in salt-stressed cells but not in control cells. In general, the levels of branched PLFAs increased more in stressed cells than in unstressed cells.

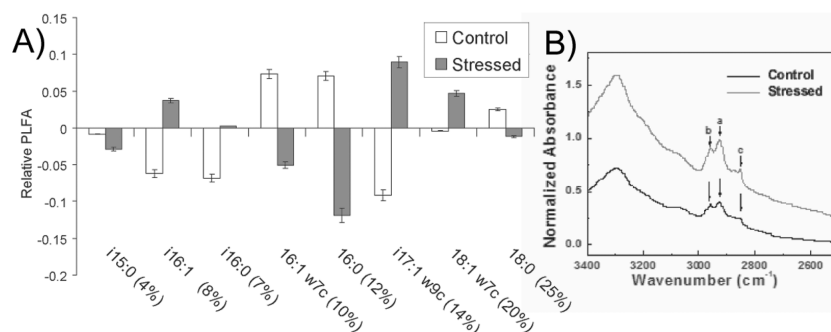The response of the PLFA profile to salt stress has been

FIG. 4. Fatty acid data. (A) Relative changes in eight major types of PLFAs after NaCl stress (data for fatty acid structures are available at http://vimss.lbl.gov/SaltStress/). Mole fractions of individual PLFAs were determined in triplicate. The data were computed as follows: $(V_1/V_0)/(C_1/C_0) - 1$, where V_1 is the value for salt-stressed cells at 120 min, V_0 is the value for salt-stressed cells at zero time, C_1 is the value for control cells at 120 min, and C_0 is the value for control cells at zero time. (B) sFTIR data for the 3,400- to 2,400-cm^{-1} window, showing changes in the peaks at 2,925 cm^{-1} (peak a), 2,958 cm^{-1} (peak b), and 2,852 cm^{-1} (peak c) that were indicative of an increase in the total lipid content in the salt-treated cells.

examined in several bacteria (31, 37). Models for lipid composition changes in both gram-positive and gram-negative bacteria have been suggested (31). *D. vulgaris* appears to exhibit the mechanisms generally found in halotolerant, gram-positive bacteria, in which an overall increase in the level of branched PLFAs, both saturated and unsaturated, is observed during salt stress. Although it is the combined ratio of different PLFAs that determines the viscosity of the resulting membrane, increases in the levels of lower-melting-temperature branched or unsaturated fatty acids are known to increase membrane fluidity (31). Similar to cold stress, salt stress is known to increase membrane rigidity (37), and increases in the levels of branched PLFAs may be the bacterial response needed to reestablish optimal membrane fluidity. Consistent with this hypothesis, unsaturation in fatty acids also increases membrane fluidity, and *Synechocystis* strains overexpressing a desaturase gene were found to be more robust under salt stress conditions (1).

The small increase in the level of lipids in the salt-stressed biomass was also observed in sFTIR experiments performed with whole cells (Fig. 4). No significant changes were found in the expression of genes encoding biosynthesis or modification functions of fatty acids or polysaccharides (http://vimss.lbl.gov/SaltStress/). However, ICAT proteomics did reveal increases in the levels of OmpH, which is putatively involved in lipopolysaccharide biosynthesis, and RfbA, which is involved cell wall biogenesis (Table 2).

Energy production. GB import, ion efflux, and helicases all require ATP hydrolysis, which may explain the significant up-regulation in F-type ATPases seen at both the transcript and protein levels (Fig. 2B and Table 2). Consistent with an increase in the energy requirement, the transcript levels for all genes (DVU0531 to DVU0536) in the operon encoding the high-molecular-weight cytochrome Hmc increased (Fig. 2B) in both NaCl and KCl stress conditions. Hmc is a potential transmembrane redox protein complex that has been reported to be involved in electron transport and energy production (25). Interestingly, expression of the Rrf12 operon (DVU0529 and DVU0530), which is located immediately downstream of the Hmc operon and is the predicted negative regulator for Hmc (32), also increased during salt stress (http://vimss.lbl.gov/SaltStress/).

Increases in transcript levels were observed for the members of the operon encoding part of the sulfate reduction pathway (DVU0846 to DVU0851) after treatment with NaCl (Table 1). Increases were also observed at the protein level for ApsA, the adenylyl sulfate reductase α subunit (DVU0847), and QmoB, the quinone-interacting membrane-bound oxidoreductase (DVU0849), although there was not significant up-regulation of QmoA (DVU0848) (Table 2). Sulfate is the terminal electron acceptor for anaerobic respiration of *D. vulgaris*. Taken together, these data indicate that there was an increase in sulfate reduction and suggest that stressed cells may require more energy than unstressed cells. In addition, the mRNA level for the sulfate permease (DVU0279) was up-regulated. This may cause a paradox for the salt-stressed cell, since this permease has been shown to function as an Na$^+$ symporter (14).

An unexplained contradiction is the apparent down-regulation of several lactate permeases in both NaCl- and KCl-stressed cells (Fig. 2A and Table 1). Additional energy requirements would be expected to require greater lactate uptake. Preliminary data from enzymatic assays performed with cell culture supernatant did not reveal a change in the lactate consumed by salt-stressed cells (data not shown), but more experiments are required to obtain a better understanding of lactate metabolism. The pyruvate metabolic pathway also appeared to be down-regulated (Fig. 2A). However, there is sufficient redundancy in the pyruvate-to-acetyl coenzyme A pathway in the genome such that this metabolic flux could have remained unchanged during salt stress.

Comparison of stress responses to Na$^+$ and K$^+$. In many bacteria, K$^+$ accumulation via the *trk* and *kdp* systems is a primary response to excess Na$^+$ ions (7, 36, 41, 54). *D. vulgaris* has four genes (DVU0412, DVU0413, DVU1606, DVU2302) that are predicted to be involved in K$^+$ uptake and transport and an operon homologous to the *E. coli kdp* K$^+$ transport system (DVU3334 to DVU3339). However, microarray data did not indicate a significant change in any of these candidates except DVU3335, a histidine sensor kinase, whose transcript level decreased with KCl stress (Table 1). Most importantly, addition of KCl did not alleviate the detrimental effect of NaCl on growth. In fact, increasing K$^+$ concentrations were found to
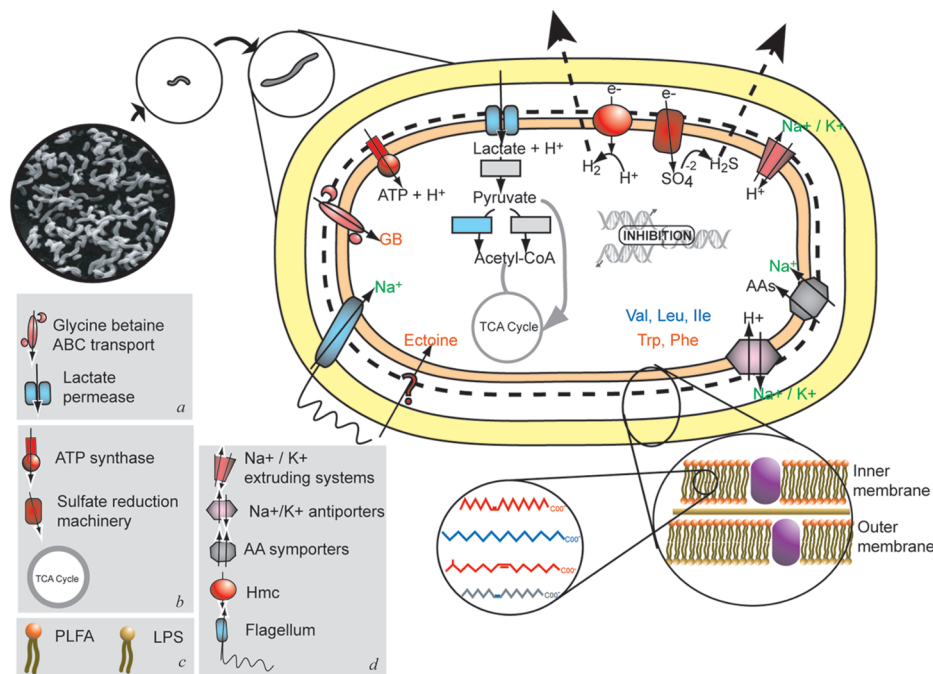
FIG. 5. Schematic diagram of molecular changes observed in *D. vulgaris* after exposure to inhibitory NaCl concentrations. Red indicates an increase, while blue indicates a decrease. Gray indicates no change. (a) Data obtained from microarray, proteomics, metabolite, and osmoprotection assays; (b) data obtained from microarray and proteomics assays; (c) data obtained from PLFA and sFTIR analyses; and (d) data obtained from only microarray analysis. Cell morphology data were obtained by electron microscopy. TCA, tricarboxylic acid; LPS, lipopolysaccharide; AA, amino acid; CoA, coenzyme A.

be additive with Na^+ for decreasing the growth rate (data not shown). Thus, at the NaCl concentration used here, uptake of K^+ ions was not an important response mechanism in *D. vulgaris*.

The overall similarity of microarray data obtained after NaCl and KCl challenges to *D. vulgaris* was striking (Fig. 2 and Table 1). Very few differences were observed, and the differences were primarily differences for hypothetical proteins whose functions are unknown. Those with homologies to products of known genes included an ABC transport protein for branched amino acids (DVU2744), and several genes for methionine and leucine biosynthesis were up-regulated only in KCl stress conditions (http://vimss.lbl.gov/SaltStress/).

Regulatory systems. Several regulons have been identified in *D. vulgaris* (51), and the most striking differential expression involved increases in gene expression for members of the ferric uptake regulon (FUR) after salt stress (Fig. 2). FUR derepression was also observed in response to heat shock (13), oxygen exposure, and acid stress (He and Zhou, unpublished data) and might be a global stress response in *D. vulgaris*. In *B. subtilis*, high salinity causes iron deficiency, leading to derepression of FUR genes, particularly siderophore biosynthesis genes (26). Possibly because of its anaerobic lifestyle, *D. vulgaris* appears to lack a siderophore biosynthetic pathway. However, even though omission of Fe^{2+} from the LS4D growth medium severely affected growth, it did not affect the net sensitivity of *D. vulgaris* to salt or the ability of GB to alleviate growth deficiency (http://vimss.lbl.gov/SaltStress/). The ability of GB to protect against salt stress in the absence of Fe^{2+} suggests that FUR may not regulate the GB uptake operon.

In bacteria, two-component systems play an important role in initiating responses to external stimuli and stress. In the cyanobacterium *Synechocystis*, a histidine kinase involved in a salt stress response has been identified (47). Microarray data for *D. vulgaris* transcripts showed that there were changes in several histidine kinases during salt stress (http://vimss.lbl.gov/SaltStress/), but further experiments are needed to confirm their specific involvement. Other regulatory proteins, such as the stationary-phase RpoS σ^{70} sigma factor, have also been reported to be involved in the salt stress response (12). Although some δ-proteobacteria apparently have a well-recognized RpoS ortholog (43), *D. vulgaris* appears not to encode RpoS. Three putative σ^{70} factors in *D. vulgaris*, *rpoD* (DVU1788), *rpoH* (DVU1584), and *fliA* (DVU3229), did not change significantly during salt stress, although σ^{54}, encoded by *rpoN* (DVU1628), appeared to be up-regulated at the transcript level (Table 1). Curiously, proteomics data also indicated that the level of RpoC, the RNA polymerase β′ subunit, increased in the salt-stressed cells (Tables 1 and 2).

Comparison of genomics data. The microarray and proteomics analyses performed in this study were targeted to study the stress response rather than adaptation. To ensure that stress was measured and also that the cells were not moribund, parallel studies were performed 2 h following salt addition. Although the maximum number of changers was observed at this time, most of the changes at the microarray level did not exceed fivefold. This is not surprising since the doubling time of *D. vulgaris* growing in LS4D medium at 30°C is 5 h. The data suggest that changes at the proteome level were even milder. Using the cysteine-tagging ICAT method, 167 proteins were identified,

and 139 of these proteins had stressed/control ratios. Of these, 79 showed changes greater than 30% and were considered to be proteins that showed a significant change (Table 2) (http://vimss.lbl.gov/SaltStress/). Twenty-seven of the changing proteins showed trends similar to trends in mRNA levels (http://vimss.lbl.gov/SaltStress/). Differences between microarray and proteomics data have been observed in most studies which used both techniques to map cellular responses (3, 13, 21, 24). Such differences may arise because of the inherent lag between mRNA changes and changes in protein levels. Posttranslational modifications and regulation, such as turnover and protein secretion, could also contribute to the differences. However, further validation is required to confirm the cause or significance of any of these differences. Additionally, while a correlation between absolute protein quantity and mRNA value may be expected (35, 58), correlations between fold changes in microarray data and proteomics data appear to be more variable (3, 13, 21, 24).

Salt stress model for *D. vulgaris* Hildenborough. The different techniques used in this study allowed us to observe the initial effects and responses to salt stress and to formulate a more complete salt stress model for a single organism (Fig. 5). Uptake of available molecules, such as GB and ectoine, from the environment is a robust strategy to counter osmotic stress and appears to be the favored mechanism in *D. vulgaris*. Upregulation at the transcript level also suggests that a variety of efflux mechanisms are involved. Cells may also utilize available protective mechanisms, such as Na^+/H^+ antiporters that are abundant but show no up-regulation upon stress. Other immediate responses include up-regulation of chemotaxis systems, apparent motility of the cells, and adjustments in cell wall composition. Increases in ATP production are supported at both the transcript and protein levels. Increases in the transcript levels of all members of the Hmc operon suggest that electron channeling may also increase during salt stress in *D. vulgaris*.

The most striking long-term effect of salt stress was the elongation of the cells, which was observed in the presence of both NaCl and KCl and was corrected by addition of GB. The elongated structures observed may have been caused by inhibition of DNA replication or may have been due to an inability to form septa. While additional experiments are required to confirm either hypothesis, our preliminary observations are more consistent with the former possibility, since the cells did not show multiple chromatin stains but rather showed dilution of total DNA and there was an increase in the protein/DNA ratio in stressed cells. The increases observed in proteins required for melting base pairs are also consistent with inhibition of DNA replication. Our growth assays showed that that uptake of osmolytes corrected these stress effects, which set the stage for further experiments to define the mechanism of osmoprotection.

REFERENCES

1. **Allakhverdiev, S. I., M. Kinoshita, M. Inaba, I. Suzuki, and N. Murata.** 2001. Unsaturated fatty acids in membrane lipids protect the photosynthetic machinery against salt-induced damage in *Synechococcus*. Plant Physiol. **125:** 1842–1853.
2. **Alm, E. J., K. H. Huang, M. N. Price, R. P. Koche, K. Keller, I. L. Dubchak, and A. P. Arkin.** 2005. The MicrobesOnline web site for comparative genomics. Genome Res. **15:**1015–1022.
3. **Baliga, N. S., M. Pan, Y. A. Goo, E. C. Yi, D. R. Goodlett, K. Dimitrov, P. Shannon, R. Aebersold, W. V. Ng, and L. Hood.** 2002. Coordinate regulation of energy transduction modules in *Halobacterium* sp. analyzed by a global systems approach. Proc. Natl. Acad. Sci. USA **99:**14913–14918.
4. **Barron, A., G. May, E. Bremer, and M. Villarejo.** 1986. Regulation of envelope protein composition during adaptation to osmotic stress in *Escherichia coli*. J. Bacteriol. **167:**433–438.
5. **Benbouzidrollet, N. D., M. Conte, J. Guezennec, and D. Prieur.** 1991. Monitoring of a *Vibrio natriegens* and *Desulfovibrio vulgaris* marine aerobic biofilm on a stainless-steel surface in a laboratory tubular flow system. J. Appl. Bacteriol. **71:**244–251.
6. **Ben-David, E. A., P. J. Holden, D. J. Stone, B. D. Harch, and L. J. Foster.** 2004. The use of phospholipid fatty acid analysis to measure impact of acid rock drainage on microbial communities in sediments. Microb. Ecol. **48:**300–315.
7. **Bhargava, S.** 2005. The role of potassium as an ionic signal in the regulation of cyanobacterium *Nostoc muscorum* response to salinity and osmotic stress. J. Basic Microbiol. **45:**171–181.
8. **Blessing, T. C., B. W. Wielinga, M. J. Morra, and S. Fendorf.** 2001. CoII-IEDTA reduction by *Desulfovibrio vulgaris* and propagation of reactions involving dissolved sulfide and polysulfides. Environ. Sci. Technol. **35:**1599–1603.
9. **Brandenburg, K., S. S. Funari, M. H. Koch, and U. Seydel.** 1999. Investigation into the acyl chain packing of endotoxins and phospholipids under near physiological conditions by WAXS and FTIR spectroscopy. J. Struct. Biol. **128:**175–186.
10. **Brandis, A., and R. K. Thauer.** 1981. Growth of *Desulfovibrio* species on hydrogen and sulphate as sole energy source. J. Gen. Microbiol. **126:**249–252.
11. **Bremer, R., and R. Kramer.** 2000. Coping with osmotic challenges: osmoregulation through accumulation and release of compatible solutes in bacteria. ASM Press, Washington, D.C.
12. **Cheville, A. M., K. W. Arnold, C. Buchrieser, C. M. Cheng, and C. W. Kaspar.** 1996. *rpoS* regulation of acid, heat, and salt tolerance in *Escherichia coli* O157:H7. Appl. Environ. Microbiol. **62:**1822–1824.
13. **Chhabra, S. R., Q. He, K. H. Huang, S. P. Gaucher, E. J. Alm, Z. He, M. Z. Hadi, T. C. Hazen, J. D. Wall, J. Zhou, A. P. Arkin, and A. K. Singh.** 2006. Global analysis of heat shock response in *Desulfovibrio vulgaris* Hildenborough. J. Bacteriol. **188:**1817–1828.
14. **Cypionka, H.** 1995. Solute transport and cell energetics. Plenum, New York, NY.
15. **Dimroth, P.** 1990. Mechanisms of sodium transport in bacteria. Philos. Trans. R. Soc. Lond. B **326:**465–477.
16. **Dudoit, S., and J. Fridlyand.** 2002. A prediction-based resampling method for estimating the number of clusters in a dataset. Genome Biol. **3:**25.
17. **Edlund, A., P. D. Nichols, R. Roffey, and D. C. White.** 1985. Extractable and lipopolysaccharide fatty acid and hydroxy acid profiles from *Desulfovibrio* species. J. Lipid Res. **26:**982–988.
18. **Fairman, M. E., P. A. Maroney, W. Wang, H. A. Bowers, P. Gollnick, T. W. Nilsen, and E. Jankowsky.** 2004. Protein displacement by DExH/D "RNA helicases" without duplex unwinding. Science **304:**730–734.
19. **Funabashi, H., T. Haruyama, M. Mie, Y. Yanagida, E. Kobatake, and M. Aizawa.** 2002. Non-destructive monitoring of *rpoS* promoter activity as stress marker for evaluating cellular physiological status. J. Biotechnol. **95:**85–93.
20. **Glaasker, E., F. S. Tjan, P. F. Ter Steeg, W. N. Konings, and B. Poolman.** 1998. Physiological response of *Lactobacillus plantarum* to salt and nonelectrolyte stress. J. Bacteriol. **180:**4718–4723.
21. **Griffin, T. J., S. P. Gygi, T. Ideker, B. Rist, J. Eng, L. Hood, and R. Aebersold.** 2002. Complementary profiling of gene expression at the transcriptome and proteome levels in *Saccharomyces cerevisiae*. Mol. Cell Proteomics **1:**323–333.
22. **Griffin, T. J., D. K. Han, S. P. Gygi, B. Rist, H. Lee, R. Aebersold, and K. C. Parker.** 2001. Toward a high-throughput approach to quantitative proteomic analysis: expression-dependent protein identification by mass spectrometry. J. Am. Soc. Mass Spectrom. **12:**1238–1246.

23. **Hadas, O., and R. Pinkas.** 1995. Sulfate reduction processes in sediments at different sites in Lake Kinneret, Israel. Microb. Ecol. **30:**55–66.

24. **Hanash, S. M., M. P. Bobek, D. S. Rickman, T. Williams, J. M. Rouillard, R. Kuick, and E. Puravs.** 2002. Integrating cancer genomics and proteomics in the post-genome era. Proteomics **2:**69–75.

25. **Heidelberg, J. F., R. Seshadri, S. A. Haveman, C. L. Hemme, I. T. Paulsen, J. F. Kolonay, J. A. Eisen, N. Ward, B. Methe, L. M. Brinkac, S. C. Daugherty, R. T. Deboy, R. J. Dodson, A. S. Durkin, R. Madupu, W. C. Nelson, S. A. Sullivan, D. Fouts, D. H. Haft, J. Selengut, J. D. Peterson, T. M. Davidsen, N. Zafar, L. Zhou, D. Radune, G. Dimitrov, M. Hance, K. Tran, H. Khouri, J. Gill, T. R. Utterback, T. V. Feldblyum, J. D. Wall, G. Voordouw, and C. M. Fraser.** 2004. The genome sequence of the anaerobic, sulfate-reducing bacterium *Desulfovibrio vulgaris* Hildenborough. Nat. Biotechnol. **22:**554–559.

26. **Hoffmann, T., A. Schutz, M. Brosius, A. Volker, U. Volker, and E. Bremer.** 2002. High-salinity-induced iron limitation in *Bacillus subtilis*. J. Bacteriol. **184:**718–727.

27. **Holman, H.-Y., K. A. Bjornstad, M. P. McNamara, M. C. Martin, W. R. McKinney, and E. A. Blakely.** 2002. Synchrotron infrared spectromicroscopy as a novel bioanalytical microprobe for individual living cells: cytotoxicity considerations. J. Biomed. Opt. **7:**417–424.

28. **Jain, N., J. Thatte, T. Braciale, K. Ley, M. O'Connell, and J. K. Lee.** 2003. Local-pooled-error test for identifying differentially expressed genes with a small number of replicated microarrays. Bioinformatics **19:**1945–1951.

29. **Jebbar, M., L. Sohn-Bosser, E. Bremer, T. Bernard, and C. Blanco.** 2005. Ectoine-induced proteins in *Sinorhizobium meliloti* include an ectoine ABC-type transporter involved in osmoprotection and ectoine catabolism. J. Bacteriol. **187:**1293–1304.

30. **Kaplan, D. L., and M. O'Donnell.** 2004. Twin DNA pumps of a hexameric helicase provide power to simultaneously melt two duplexes. Mol. Cell **15:**453–465.

31. **Kates, M.** 1986. Influence of salt concentration on the membrane lipids of halophilic bacteria. FEMS Microbiol. Rev. **39:**95–101.

32. **Keon, R. G., R. Fu, and G. Voordouw.** 1997. Deletion of two downstream genes alters expression of the *hmc* operon of *Desulfovibrio vulgaris* subsp. *vulgaris* Hildenborough. Arch. Microbiol. **167:**376–383.

33. **Ko, R., L. T. Smith, and G. M. Smith.** 1994. Glycine betaine confers enhanced osmotolerance and cryotolerance on *Listeria monocytogenes*. J. Bacteriol. **176:**426–431.

34. **Li, X., Z. He, and J. Zhou.** 2005. Selection of optimal oligonucleotide probes for microarrays using multiple criteria, global alignment and parameter estimation. Nucleic Acids Res. **33:**6114–6123.

35. **Liu, H., R. G. Sadygov, and J. R. Yates, 3rd.** 2004. A model for random sampling and estimation of relative protein abundance in shotgun proteomics. Anal. Chem. **76:**4193–4201.

36. **Liu, Y., W. Gao, Y. Wang, L. Wu, X. Liu, T. Yan, E. Alm, A. Arkin, D. K. Thompson, M. W. Fields, and J. Zhou.** 2005. Transcriptome analysis of *Shewanella oneidensis* MR-1 in response to elevated salt conditions. J. Bacteriol. **187:**2501–2507.

37. **Los, D. A., and N. Murata.** 2004. Membrane fluidity and its roles in the perception of environmental signals. Biochim. Biophys. Acta **1666:**142–157.

38. **Lovley, D. R., and E. J. P. Phillips.** 1994. Reduction of chromate by *Desulfovibrio vulgaris* and its c_3 cytochrome. Appl. Environ. Microbiol. **60:**726–728.

39. **Ma, D., D. N. Cook, M. Alberti, N. G. Pon, H. Nikaido, and J. E. Hearst.** 1995. Genes *acrA* and *acrB* encode a stress-induced efflux system of *Escherichia coli*. Mol. Microbiol. **16:**45–55.

40. **MacKay, V. L., X. Li, M. R. Flory, E. Turcott, G. L. Law, K. A. Serikawa, X. L. Xu, H. Lee, D. R. Goodlett, R. Aebersold, L. P. Zhao, and D. R. Morris.** 2004. Gene expression analyzed by high-resolution state array analysis and quantitative proteomics: response of yeast to mating pheromone. Mol. Cell Proteomics **3:**478–489.

41. **Matsuda, N., H. Kobayashi, H. Katoh, T. Ogawa, L. Futatsugi, T. Nakamura, E. P. Bakker, and N. Uozumi.** 2004. Na$^+$-dependent K$^+$ uptake Ktr system from the cyanobacterium *Synechocystis* sp. PCC 6803 and its role in the early phases of cell adaptation to hyperosmotic shock. J. Biol. Chem. **279:**54952–54962.

42. **Noguera, D. R., G. A. Brusseau, B. E. Rittmann, and D. A. Stahl.** 1998. Unified model describing the role of hydrogen in the growth of *Desulfovibrio vulgaris* under different environmental conditions. Biotechnol. Bioeng. **59:**732–746.

43. **Nunez, C., L. Adams, S. Childers, and D. R. Lovley.** 2004. The RpoS sigma factor in the dissimilatory Fe(III)-reducing bacterium *Geobacter sulfurreducens*. J. Bacteriol. **186:**5543–5546.

44. **Nyyssola, A., T. Reinikainen, and M. Leisola.** 2001. Characterization of glycine sarcosine *N*-methyltransferase and sarcosine dimethylglycine *N*-methyltransferase. Appl. Environ. Microbiol. **67:**2044–2050.

45. **Ouattara, A. S., and V. A. Jacq.** 1992. Characterization of sulfate-reducing bacteria isolated from senegal ricefields. FEMS Microbiol. Ecol. **101:**217–228.

46. **Padan, E., and T. A. Krulwich.** 2000. Sodium stress in bacterial stress response. ASM Press, Washington, D.C.

47. **Paithoonrangsarid, K., M. A. Shoumskaya, Y. Kanesaki, S. Satoh, S. Tabata, D. A. Los, V. V. Zinchenko, H. Hayashi, M. Tanticharoen, I. Suzuki, and N. Murata.** 2004. Five histidine kinases perceive osmotic stress and regulate distinct sets of genes in *Synechocystis*. J. Biol. Chem. **279:**53078–53086.

48. **Panepinto, J., L. Liu, J. Ramos, X. Zhu, T. Valyi-Nagy, S. Eksi, J. Fu, H. A. Jaffe, B. Wickes, and P. R. Williamson.** 2005. The DEAD-box RNA helicase Vad1 regulates multiple virulence-associated genes in *Cryptococcus neoformans*. J. Clin. Investig. **115:**632–641.

49. **Pfenninger-Li, X., S. Albracht, R. van Belzen, and P. Dimroth.** 1996. NADH: ubiquinone oxidoreductase of *Vibrio alginolyticus*: purification, properties, and reconstitution of the Na$^+$ pump. Biochemistry **35:**6233–6242.

50. **Postgate, J. R.** 1984. The sulfate-reducing bacteria. Cambridge University Press, Cambridge, United Kingdom.

51. **Rodionov, D. A., I. Dubchak, A. Arkin, E. Alm, and M. S. Gelfand.** 2004. Reconstruction of regulatory and metabolic pathways in metal-reducing delta-proteobacteria. Genome Biol. **5:**R90.

52. **Sanan-Mishra, N., X. H. Pham, S. K. Sopory, and N. Tuteja.** 2005. Pea DNA helicase 45 overexpression in tobacco confers high salinity tolerance without affecting yield. Proc. Natl. Acad. Sci. USA **102:**509–514.

53. **Shapiguzov, A., A. A. Lyukevich, S. I. Allakhverdiev, T. V. Sergeyenko, I. Suzuki, N. Murata, and D. A. Los.** 2005. Osmotic shrinkage of cells of *Synechocystis* sp. PCC 6803 by water efflux via aquaporins regulates osmo-stress-inducible gene expression. Microbiology **151:**447–455.

54. **Sleator, R. D., and C. Hill.** 2002. Bacterial osmoadaptation: the role of osmolytes in bacterial stress and virulence. FEMS Microbiol. Rev. **26:**49–71.

55. **Steil, L., T. Hoffmann, I. Budde, U. Volker, and E. Bremer.** 2003. Genome-wide transcriptional profiling analysis of adaptation of *Bacillus subtilis* to high salinity. J. Bacteriol. **185:**6358–6370.

56. **Steuber, J., C. Schmid, M. Rufibach, and P. Dimroth.** 2000. Na$^+$ translocation by complex I (NADH:quinone oxidoreductase) of *Escherichia coli*. Mol. Microbiol. **35:**428–434.

57. **Tabak, H. H., and R. Govind.** 2003. Advances in biotreatment of acid mine drainage and biorecovery of metals. 2. Membrane bioreactor system for sulfate reduction. Biodegradation **14:**437–452.

58. **Wang, R., J. T. Prince, and E. M. Marcotte.** 2005. Mass spectrometry of the *M. smegmatis* proteome: protein expression levels correlate with function, operons, and codon bias. Genome Res. **15:**1118–1126.

59. **Wei, J., J. Sun, W. Yu, A. Jones, P. Oeller, M. Keller, G. Woodnutt, and J. M. Short.** 2005. Global proteome discovery using an online three-dimensional LC-MS/MS. J. Proteome Res. **4:**801–808.

60. **White, C., R. J. Bobbie, J. D. King, J. S. Nickels, and P. Amoe.** 1979. Lipid analysis of sediments for microbial biomass and community structure. American Society of Testing and Materials, Philadelphia, PA.

61. **Wolters, D. A., M. P. Washburn, and J. R. Yates, 3rd.** 2001. An automated multidimensional protein identification technology for shotgun proteomics. Anal. Chem. **73:**5683–5690.

62. **Ye, Q., Y. Roh, S. L. Carroll, B. Blair, J. Zhou, C. L. Zhang, and M. W. Fields.** 2004. Alkaline anaerobic respiration: isolation and characterization of a novel alkaliphilic and metal-reducing bacterium. Appl. Environ. Microbiol. **70:**5595–5602.